Impurity effects at finite temperature in the two-dimensional $S=1/2$ Heisenberg antiferromagnet

Kaj H. Höglund[1] and Anders W. Sandvik[1,2]
[1]*Department of Physics, Åbo Akademi University, Porthansgatan 3, FIN-20500, Turku, Finland*
[2]*Department of Physics, Boston University, 590 Commonwealth Avenue, Boston, Massachusetts 02215, USA*
(Received 6 February 2004; published 12 July 2004)

We discuss effects of various impurities on the magnetic susceptibility and the specific heat of the quantum $S=1/2$ Heisenberg antiferromagnet on a two-dimensional square lattice. For impurities with spin $S_i>0$ (here $S_i=1/2$ in the case of a vacancy or an added spin, and $S_i=1$ for a spin coupled ferromagnetically to its neighbors), our quantum Monte Carlo simulations confirm a classical-like Curie susceptibility contribution $S_i^2/3T$, which originates from an alignment of the impurity spin with the local Néel order. In addition, we find a logarithmically divergent contribution, which we attribute to fluctuations transverse to the local Néel vector. We also study frustrated and nonfrustrated bond impurities with $S_i=0$. For a simple intuitive picture of the impurity problem, we discuss an effective few-spin model that can distinguish between the different impurities and reproduces the leading-order simulation data over a wide temperature range.

DOI: 10.1103/PhysRevB.70.024406 PACS number(s): 75.10.Jm, 75.10.Nr, 75.40.Cx, 75.40.Mg

I. INTRODUCTION

The problem of impurities in low-dimensional quantum antiferromagnets has attracted considerable attention ever since the discovery of high-temperature superconductivity in the cuprates.[1] At low concentration, holes doped into the CuO_2 planes are localized, or have very low mobility, and hence static impurities are relevant for understanding the initial reduction of antiferromagnetism upon doping compounds such as La_2CuO_4. These impurities are expected to be magnetically frustrated.[2] Although not directly related to the breakdown of antiferromagnetism associated with the onset of superconductivity, static nonfrustrating impurities, e.g., inert holes corresponding to substitution of Cu atoms by nonmagnetic Zn,[3,4] also can give important information pertaining to the nature of the interactions in the CuO_2 planes. The same applies to related cuprates where the planes are broken up into chains[5] or ladders.[6] Very recently, similar impurity problems were also suggested to be of relevance to possible physical realizations of quantum computers.[7]

On the theoretical side, Heisenberg impurity models can be studied by a wide range of modern quantum many-body methods. Importantly, numerical techniques, such as quantum Monte Carlo and the density matrix renormalization group, can give approximation-free results against which analytical approaches can be tested on a quantitative level. Once such a program has been completed, the applicability of a Heisenberg description to an experimental system can be judged without concerns about approximations in the calculations. There is already a large body of work devoted to various impurity effects, and a coherent picture is emerging. Restricting ourselves to work on single impurities, we note several ground state calculations for Heisenberg chains,[8–11] ladders,[12–14] and the two-dimensional (2D) square lattice.[13,15–22] Extensive work on chains[23–25] and 2D systems[21,26–29] at finite temperature has also been carried out. In this paper, we continue our studies[27] of finite-temperature effects of isolated static impurities in the standard 2D Heisenberg model, and also present some results for the 3D system.

In a recent comprehensive quantum field-theoretical work,[21] a low-temperature theory of an arbitrary quantum impurity in a 2D antiferromagnetic host system was developed, with the host being either in the $T=0$ magnetically ordered phase (i.e., in the renormalized-classical regime at $T>0$) or close to a quantum-critical point. In the magnetically ordered phase a leading-order classical-like Curie contribution to the impurity susceptibility was predicted to stem from the coupling of the impurity moment $\mathbf{S}_i$ to the local Néel order as the temperature $T\to 0$, i.e., $\chi^z_{\rm imp}\to S_i^2/3T$. Stimulated in part by these theoretical predictions by Sachdev *et al.*,[21] we recently carried out a large-scale quantum Monte Carlo (QMC) study [27] of the 2D $S=1/2$ Heisenberg antiferromagnet and confirmed the Curie prefactor $1/12$ in the renormalized-classical regime, for a vacancy (missing spin) as well as for an added $S_i=1/2$ impurity spin. However, we also discovered a low-T logarithmically divergent subleading contribution to the impurity susceptibility. This anomaly was attributed to the transverse component, for which a T-independent behavior had been predicted.[21,30] Related logarithmic divergences had also previously been found, e.g., in an exact study of an impurity in the classical 2D Heisenberg model,[31] and in a Green's function treatment of the 2D quantum model with an extra spin at $T=0$.[16] In the latter study, the frequency dependent transverse impurity susceptibility $\chi^{\perp}_{\rm imp}(T=0,\omega)$ was found to be log divergent when $\omega\to 0$. More recently, an anomalous susceptibility was also found in the Heisenberg model with a finite impurity concentration.[32]

Recent efforts, by Sachdev and Vojta[28] and Sushkov,[29] to explain our previous numerical findings,[27] have resulted in more complete field-theoretical descriptions where the impurity susceptibility indeed acquires a previously unnoticed subleading log divergent contribution. Its principal cause can also in these analytical treatments be considered as associated with the transverse component, although there are also higher-order logarithmic contributions arising from longitudinal fluctuations.[28,30] In the formulation by Sachdev and Vojta,[28] which relies on an expansion of the nonlinear σ

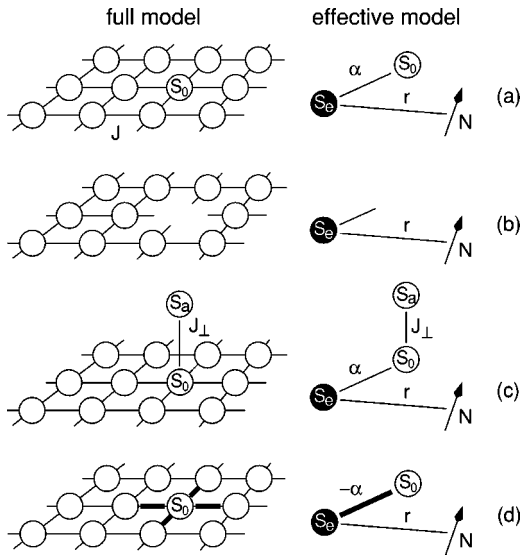

FIG. 1. Full Heisenberg models and corresponding effective models of the (a) pure, (b) vacancy, (c) added-spin, and (d) four ferromagnetic bonds systems. Thick solid lines symbolize ferromagnetic spin-spin couplings $-J_F<0$, with $J_F=J$. The free parameters of the effective models are the couplings α and r.

model around dimensionality $d=1$, a very detailed form for the logarithmic corrections to the impurity susceptibility was given. For general impurity spin S_i:

$$\chi^z_{\rm imp} = \frac{S_i^2}{3T}\left[1 + \frac{T}{\pi\rho_s}\ln\left(\frac{C_1\rho_s}{T}\right) - \frac{T^2}{2\pi^2\rho_s^2}\ln\left(\frac{C_2\rho_s}{T}\right) + O\left(\frac{T}{\rho_s}\right)^3\right], \tag{1}$$

where ρ_s is the spin stiffness of the bulk-ordered antiferromagnet in the absence of impurities and the unknown constants $C_{1,2}$ are in general nonuniversal, but become universal when a quantum critical point is approached. The first subleading term $\propto\ln(1/T)$ in Eq. (1) hence accounts for the log divergent behavior observed in our numerical studies. The quantitative agreement between Eq. (1) and our numerical data is quite remarkable, as will be shown in this paper. Our results also agree qualitatively with the analytical results obtained by Sushkov.[29]

The purpose of this paper is to give a more complete numerical account of the effects of different types of single static impurities on the magnetic susceptibility of the 2D $S=1/2$ Heisenberg antiferromagnet on a square lattice. Some of the results were previously summarized in Ref. 27. The impurity effects were there determined for a vacancy and an added-spin impurity, by calculating impurity susceptibilities with the stochastic series expansion (SSE) QMC technique.[33,34] The impurity susceptibility is simply the difference between the susceptibilities of the pure and doped Heisenberg models. In this paper we compare our numerical results for the vacancy and added-spin impurity models with the theoretical expression in Eq. (1). We also consider an impurity consisting of a spin coupled ferromagnetically to its four nearest neighbors [see Fig. 1(d)]. This coupling arrangement is nonfrustrating and can be expected to lead to an $S_i=1$ impurity, in contrast to the $S_i=1/2$ vacancy and added-spin impurities. It was suggested by Aharony *et al.*,[2] that hole doping the parent compounds of the cuprate superconductors could lead to effective frustrated ferromagnetic exchange couplings between nearest neighbor Cu spins. Motivated by this scenario, we have also considered an impurity model with a single ferromagnetic bond, and compared this with a missing bond. The 2D Heisenberg antiferromagnet with two vacancies on different sublattices, and at different separations, is also studied in order to further elucidate the behavior of the single-vacancy impurity susceptibility. Finally, we have considered a single vacancy in the three-dimensional (3D) Heisenberg antiferromagnet, for which analytical limiting expressions has also been obtained recently. [28] Although the main focus of this paper is on the susceptibility, we will also present some results for impurity effects on the internal energy and the specific heat.

In Ref. 27 we also introduced effective models for the vacancy and added-spin systems. These models are very simple few-spin systems constructed in order to capture the leading-order impurity effects—they do not contain the log corrections. They provide simple physical pictures of the dominant mechanisms at play in the full Heisenberg impurity models. In this paper the effective models are discussed in detail, and the concept is further demonstrated by results for added-spin impurities with different couplings to the host and the ferromagnetically coupled in-plane impurity spin.

The rest of the paper is organized as follows: In Sec. II the full Heisenberg and effective models, as well as their impurity susceptibilities, are defined. In Sec. III the SSE Monte Carlo method is briefly outlined, and the improved estimators needed to achieve sufficient statistical accuracy are discussed. We also describe an averaging trick used to alleviate the sign problem in our study of the frustrated ferromagnetic-bond impurity. The SSE results are presented and compared with the corresponding effective models in Sec. IV. Concluding remarks are given in Sec. V. In the Appendix we discuss the specific heat of the pure Heisenberg model, for which we have obtained low-temperature results of unprecedented accuracy. In order to provide benchmark results for other calculations, we also list some selected high-precision numerical values for energies and susceptibilities of systems with different impurities.

II. IMPURITY MODELS AND SUSCEPTIBILITIES

Following Ref. 21, an impurity susceptibility is defined as the difference between the susceptibility of an impurity system and the pure system, i.e.,

$$\chi^{z,(i)}_{\rm imp} = \chi^z_{(i)} - \chi^z_{(a)}, \tag{2}$$

where $i=b,c,d,e$, and f, correspond to the different impurity systems shown in Figs. 1 and 2, and $\chi^z_{(a)}$ is the susceptibility of the pure system. The susceptibilities on the right-hand side of Eq. (2) are not normalized by the system size, i.e.,

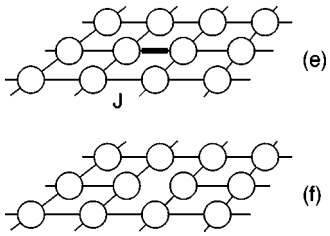

FIG. 2. Full Heisenberg models of the (e) frustrating ferromagnetic bond ($J_F=J$) and (f) removed bond ($J_F=0$) systems.

$$\chi^z_{(i)} = \frac{1}{T}\left(\sum_j S^z_j\right)^2, \tag{3}$$

where the sum is over all the spins of the pure or impurity systems. The impurity susceptibilities are hence intensive differences of extensive quantities, and they provide a natural framework for quantifying the effects of different isolated impurities on the susceptibility of the pure system. They also give the leading (linear) dependence on the concentration of impurities. The definition in Eq. (2) will be used both in the context of the full Heisenberg models and the corresponding effective models, both of which will be defined in this section. Quantities analogous to Eq. (2) will also be used for the internal energy and the specific heat.

The impurity susceptibility can be separated in components parallel and perpendicular to a given direction. Here the separation is done with respect to an axis along the orientation of the local Néel order at the impurity. In the isotropic 2D Heisenberg antiferromagnet, true long-range Néel order sets in, i.e., the spin-rotation symmetry of an infinite system is broken, only at $T=0$.[36] The components $\chi^{\parallel,(i)}_{\rm imp}$ and $\chi^{\perp,(i)}_{\rm imp}$, where $\parallel$ and $\perp$ refer to directions parallel and perpendicular to the Néel order, are, therefore, true physical observables only at $T=0$. However, our calculations show a temperature behavior that confirms an approximate, but conceptually useful, separation of the impurity susceptibility in components already at low finite T, as will be shown in Sec. IV. In the 3D Heisenberg antiferromagnet, Néel order is present already at finite temperature, below $T_c/J\approx 0.95$,[35] which makes the two components truly distinguishable. The effective impurity models are defined to include a fluctuating direction given by a classical vector **N**, describing a local Néel order with respect to which susceptibility components can be defined. Comparisons with the QMC results show that the separation into components is useful even at a quantitative level.

A. Full Heisenberg models

The basis for this study is the isotropic $S=1/2$ Heisenberg antiferromagnet on a periodic $L\times L$ lattice. This model is defined by the Hamiltonian

$$H_{(a)} = J\sum_{b=1}^{N_b} \mathbf{S}_{i(b)}\cdot\mathbf{S}_{j(b)}, \tag{4}$$

where $J>0$, bond b connects the nearest-neighbor sites $[i(b),j(b)]$, and N_b is the total number of bonds. $H_{(a)}$ is given a pictorial representation to the left in Fig. 1(a), and will hereafter be referred to as the full Hamiltonian of the pure system. Impurity models are obtained by introducing single defects in the pure model.

We begin by presenting the models with impurity moments $S_i\neq 0$. They are illustrated in Fig. 1. When a single spin $\mathbf{S}_0$ is removed from the square lattice, the vacancy model shown to the left in Fig. 1(b) is obtained. We will study it in 2D as well as in 3D. The added-spin model, shown to the left in Fig. 1(c), is obtained by coupling a single off-plane spin-$\frac{1}{2}$ $\mathbf{S}_a$ antiferromagnetically to a spin $\mathbf{S}_0$ on the square lattice. Two different values on the coupling strength $J_\perp=J$ and $J_\perp=J/2$ will be considered here. In the limit $J_\perp\to\infty$, the magnetic properties of the added-spin model become equivalent to the vacancy model, since the two spins $\mathbf{S}_a$ and $\mathbf{S}_0$ are then locked in a singlet state. An $S_i=1$ impurity is obtained by considering a configuration of four ferromagnetic bonds with one spin in common, as shown in Fig. 1(d).

We also consider the models with impurity moments $S_i=0$ shown in Fig. 2. A system with one frustrating ferromagnetic bond, where the spin-spin coupling is $-J_F<0$, is shown in Fig. 2(e). In the limit $J_F/J\to\infty$, one might hence expect a corresponding $S_i=1$ impurity moment, as the two spins connected by the ferromagnetic bond then form a triplet. On the other hand, for $J_F=0$ clearly $S_i=0$, and hence a transition between $S_i=0$ and 1 might be expected at some intermediate J_F. However, it has been shown that in a Néel ordered bulk, the correlations between the spins connected by the ferromagnetic bond remain antiferromagnetic,[17] which is possible because of the broken degeneracy of the triplet when it is coupled to an asymmetric environment. Hence, counterintuitively, an $S_i=1$ behavior when $T\to 0$ may actually never be realized with a ferromagnetic bond impurity. We will here consider only the coupling strength $J_F=J$, for which the sign problem due to frustration can be alleviated by a position averaging procedure, as discussed in Sec. III. Our QMC data shows that the impurity moment $S_i=0$ in this case, and the behavior is similar to the removed-bond impurity model ($J_F=0$) shown in Fig. 2(f).

Two-impurity models are useful for further clarifying the properties of the single-impurity models. Here we will consider only the case of two vacancies, which are chosen to be either at a fixed short distance from each other or maximally separated on the $L\times L$ square lattice.

B. Effective models

The purpose of introducing effective models is to capture the dominant mechanisms at play in the full Heisenberg models with very simple systems containing a minimal number of adjustable parameters. The effective models are constrained by two criteria: (i) they should reproduce the high-T impurity susceptibility, the sign of which depends on whether a spin has been added or removed, and (ii) they should mimic the expected[21] leading-order behavior $S_i^2/3T$ of the impurity susceptibilities at low T, i.e., the alignment of the impurity moment with the local Néel order. Effective models are here considered for the full $S_i\neq 0$ impurity models shown in Fig. 1.

In our effective models the local Néel order at the impurity is modeled by a classical "nonmagnetic" vector **N**. When a single spin $\mathbf{S}_0$ is removed from the full model of the pure system, as shown to the left in Fig. 1(b), the remaining system has an $S=1/2$ ground state due to the sublattice asymmetry. Hence, the effective model corresponding to the vacancy system, shown to the right in Fig. 1(b), is simply defined with a single effective remnant "environment" spin-$\frac{1}{2}$ $\mathbf{S}_e$. This spin is coupled to a classical unit vector **N** representing the orientation of the local Néel order. The magnitude of this order is absorbed in the coupling strength r. The effective model for the pure system is naturally obtained by reinserting the spin $\mathbf{S}_0$, as shown to the right in Fig. 1(a), with $\alpha>0$ for antiferromagnetic coupling. The effective model for the added-spin system, shown to the right in Fig. 1(c), is obtained by coupling an extra spin-$\frac{1}{2}$ $\mathbf{S}_a$ to $\mathbf{S}_0$. Finally, the effective model for the system with a configuration of four ferromagnetic bonds, shown to the right in Fig. 1(d), is obtained by simply changing the sign of α, i.e., by making the coupling ferromagnetic instead of antiferromagnetic. To summarize, the Hamiltonians of the effective models, corresponding to the full models in Fig. 1, are

$$H_{(a)}^{\mathrm{eff}} = r\mathbf{N}\cdot\mathbf{S}_e + \alpha\mathbf{S}_0\cdot\mathbf{S}_e, \tag{5a}$$

$$H_{(b)}^{\mathrm{eff}} = r\mathbf{N}\cdot\mathbf{S}_e, \tag{5b}$$

$$H_{(c)}^{\mathrm{eff}} = r\mathbf{N}\cdot\mathbf{S}_e + \alpha\mathbf{S}_0\cdot\mathbf{S}_e + J_\perp\mathbf{S}_a\cdot\mathbf{S}_0, \tag{5c}$$

$$H_{(d)}^{\mathrm{eff}} = r\mathbf{N}\cdot\mathbf{S}_e - \alpha\mathbf{S}_0\cdot\mathbf{S}_e. \tag{5d}$$

The parameters $r>0$ and $\alpha>0$ cannot be derived in any trivial way. The magnitude of r should in principle depend on T, but the T dependence can be expected to be weak once the amplitude of the order has developed locally close to the impurity. One could also argue that a direct coupling between **N** and the central spin $\mathbf{S}_0$ should be included. Such a coupling is clearly mediated through the four nearest neighbors of $\mathbf{S}_0$. However, in the spirit of keeping the models as simple as possible, we here chose to accomplish this coupling indirectly through the remnant environment spin $\mathbf{S}_e$. One can further anticipate that the optimum values for the couplings r and α will depend on the impurity type, since the effective impurity spin is spread out and its coupling is mediated through the local environment of $\mathbf{S}_0$, which will be distorted in different ways by different impurities. However, we will show that the same parameters, $r/J\approx 1.90$ and $\alpha/J\approx 2.25$,[37] actually give an overall reasonable agreement for all the $S_i>0$ impurity types considered here.

The procedure for determining the susceptibilities of the effective models is straightforward. An external applied field $\mathbf{h}=h_z\mathbf{e}_z$ defines the z direction. The magnetization operators $\mathbf{M}_{(i)}$, corresponding to the effective Hamiltonians in Eqs. (5), have the z components $M_{(a)}^z=S_0^z+S_e^z$, $M_{(b)}^z=S_e^z$, $M_{(c)}^z=S_a^z+S_0^z+S_e^z$, and $M_{(d)}^z=M_{(a)}^z$. The susceptibilities are given by the usual formula

$$\chi_{(i)}^z = \left.\frac{\partial\langle\langle M_{(i)}^z\rangle\rangle_{\mathbf{N}}}{\partial h_z}\right|_{h_z=0} = \int_0^{1/T} d\tau\langle\langle M_{(i)}^z(\tau)M_{(i)}^z(0)\rangle\rangle\mathbf{N} - \frac{1}{T}\langle\langle M_{(i)}^z\rangle\rangle_{\mathbf{N}}^2, \tag{6}$$

where $i=a,b,c$, and d. Here the inner brackets $\langle\cdot\rangle$ indicate the quantum mechanical expectation value for a fixed direction of **N**, and $\langle\cdot\rangle_{\mathbf{N}}$ denotes the classical orientation average. The imaginary-time evolved operator $M_{(i)}^z(\tau) = \exp(\tau H_{(i)}^{\mathrm{eff}})M_{(i)}^z\exp(-\tau H_{(i)}^{\mathrm{eff}})$. Expressing $M_{(i)}^z$ in the coordinate system defined by **N**,

$$M_{(i)}^z = \cos(\Theta)M_{(i)}^{\parallel} - \sin(\Theta)M_{(i)}^{\perp}, \tag{7}$$

where $\parallel$ and $\perp$ denote the directions parallel and perpendicular to **N**, the expectation values can be easily calculated. The second term in Eq. (6) vanishes. The first term can be separated into components:

$$\chi_{(i)}^z = \tfrac{1}{3}\chi_{(i)}^{\parallel} + \tfrac{2}{3}\chi_{(i)}^{\perp}, \tag{8}$$

where the prefactors originate from the classical orientation averaging. The susceptibility components are

$$\chi_{(i)}^{\parallel} = \int_0^{1/T} d\tau\langle M_{(i)}^{\parallel}(\tau)M_{(i)}^{\parallel}(0)\rangle = \frac{1}{T}\langle(M_{(i)}^{\parallel})^2\rangle, \tag{9a}$$

$$\chi_{(i)}^{\perp} = \int_0^{1/T} d\tau\langle M_{(i)}^{\perp}(\tau)M_{(i)}^{\perp}(0)\rangle, \tag{9b}$$

which can be easily evaluated in the $\parallel$ basis. In this basis Eq. (9a) has the simple form because $[H_{(i)}^{\mathrm{eff}},M_{(i)}^{\parallel}]=0$.

A dominant feature of the effective models is the alignment of a quantum spin with a classical vector. This can be appreciated by examining the simple effective Hamiltonian $H_{(b)}^{\mathrm{eff}}$, given in Eq. (5b), for the vacancy system. The corresponding susceptibility is given by

$$\chi_{(b)}^z = \tfrac{1}{3}\chi_{(b)}^{\parallel} + \tfrac{2}{3}\chi_{(b)}^{\perp} = \frac{1}{3}\frac{1}{4T} + \frac{2}{3}\frac{1}{2r}\tanh\left(\frac{r}{2T}\right). \tag{10}$$

The temperature dependence of the two components is graphed in Fig. 3(b) for $r=1.90$. Since $S_e=1/2$ in this model, the $\parallel$ component can be written as $(1/3)\chi_{(b)}^{\parallel}=S_e{}^2/3T$. Hence, the classical Curie prefactor $S_e{}^2$, instead of the usual quantum mechanical prefactor $S_e(S_e+1)$, is a consequence of the finite coupling between the spin $\mathbf{S}_e$ and the classical vector **N**. This is precisely the low-T leading order behavior proposed[21] in Eq. (1) in the renormalized classical regime of a 2D antiferromagnet. The perpendicular component in Eq. (10) tends to a constant at low T. On the other hand, in the limit $r\to 0$, i.e., when $\mathbf{S}_e$ and **N** decouple, $\mathbf{S}_e$ recovers its quantum identity and the susceptibility has the usual Curie form $\chi_{(b)}^z\to S_e(S_e+1)/3T$.

The effective models also serve the purpose of elucidating the steps in determining the impurity susceptibility $\chi_{\mathrm{imp}}^{z,(b)} = \chi_{(b)}^z - \chi_{(a)}^z$. The separation in components of the susceptibility for the effective pure system, $\chi_{(a)}^z$, is shown in Fig. 3(a).

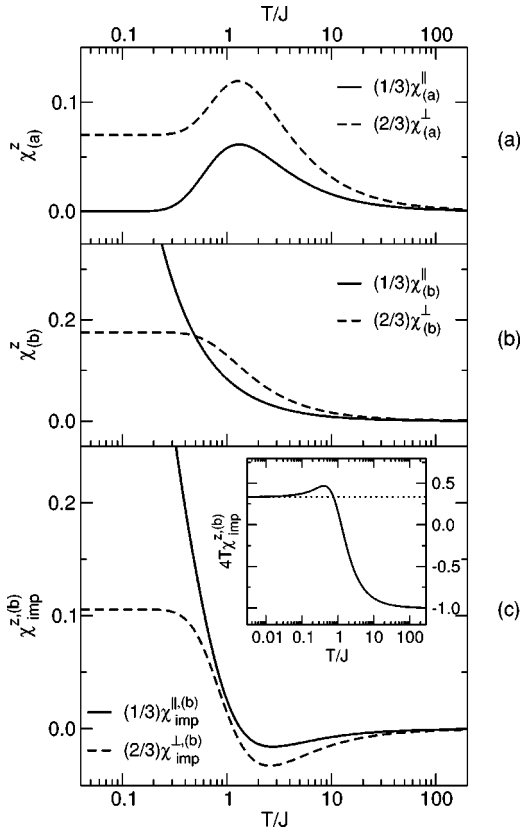

FIG. 3. The components of the susceptibilities of the effective models for the pure (a) and vacancy (b) systems. The components of the impurity susceptibility $\chi^{z,(b)}_{\rm imp}=\chi^{z}_{(b)}-\chi^{z}_{(a)}$ are shown in (c). The inset shows the $4T\chi^{z,(b)}_{\rm imp}\sim 1/3$ behavior as $T\to 0$.

The parallel component $(1/3)\chi^{\parallel}_{(a)}$ vanishes at low T since the spins $\mathbf{S}_0$ and $\mathbf{S}_e$ are then aligned antiferromagnetically with respect to $\mathbf{N}$. The perpendicular component $(2/3)\chi^{\perp}_{(a)}$ assumes a constant value at low T. The components of the susceptibility $\chi^{z}_{(b)}$ for the vacancy system were given analytically in Eq. (10) and are shown in Fig. 3(b). Finally, the components of the impurity susceptibility are shown in Fig. 3(c). At high T, the impurity susceptibility is just the sum of the Curie contributions of each independent spin, i.e., $\chi^{z,(b)}_{\rm imp}\to 1/4T-2/4T=-1/4T$. At low T the parallel component diverges, while the perpendicular component becomes a constant. The inset verifies that the parallel component is responsible for the ${S_e}^2/3T$ behavior, since $4T\chi^{z,(b)}_{\rm imp}\sim 1/3$ as $T\to 0$. Besides being capable of reproducing the expected low-T leading order behavior of the full models, the effective models also account quite accurately for impurity specific behavior at intermediate T, as will be shown in Sec. IV. There we also demonstrate that the effective models account accurately for the T dependence of the internal energy.

III. QUANTUM MONTE CARLO METHOD

The numerical method employed here for the full Heisenberg models is the operator-loop formulation of the stochastic series expansion (SSE) QMC method. It is a method based on importance sampling of the terms of the Taylor series for the density matrix. Its application to the Heisenberg model has been discussed in detail, e.g., in Refs. 33 and 34. The method is only briefly outlined here in order to discuss some important aspects of the impurity work, including a trick for alleviating the sign problem for the frustrated-bond system and the use of improved estimators for reducing statistical errors.

The Hamiltonian of the Heisenberg antiferromagnet in Eq. (4) can be cast into the form

$$H_{(a)}=-\frac{J}{2}\sum_{b=1}^{N_b}(H_{1,b}-H_{2,b})+\frac{JN_b}{4}, \tag{11}$$

where the operators $H_{1,b}$ and $H_{2,b}$, defined by

$$H_{1,b}=2\left(\tfrac{1}{4}-S^z_{i(b)}S^z_{j(b)}\right), \tag{12a}$$

$$H_{2,b}=S^+_{i(b)}S^-_{j(b)}+S^-_{i(b)}S^+_{j(b)}, \tag{12b}$$

are diagonal and off-diagonal, respectively, in the basis $\{|\alpha\rangle=|S^z_1,S^z_2,\ldots,S^z_N\rangle\}$ used in the simulation. An exact expression for the partition function Z is obtained by expanding the density matrix $e^{-\beta H}$ in a Taylor series at inverse temperature $\beta=1/T$ ($k_B=1$). The series can be truncated at some expansion power $n_{\rm max}=M$, since terms of order greater than $n\propto N\beta$ give an exponentially vanishing contribution.[33] The truncated partition function is then given by

$$Z=\sum_{\alpha}\sum_{S_M}W(\alpha,S_M)\left\langle\alpha\left|\prod_{i=1}^{M}H_{a_i,b_i}\right|\alpha\right\rangle. \tag{13}$$

Since the matrix element of the operator product takes the values 0 or 1, the statistical weight of a contributing configuration is[33]

$$W(\alpha,S_M)=\frac{(-1)^{n_2}(\beta J)^n(M-n)!}{2^n M!}. \tag{14}$$

A number of $M-n$ identity operators $H_{0,0}=I$ have been inserted in the matrix element of each term in Eq. (13), with expansion order $n<M$, and the change in prefactor reflects the number of different ways to distribute the n Hamiltonian operators among the M positions. The symbol S_M denotes a sequence of operator indices,

$$S_M=(a_1,b_1),(a_2,b_2),\ldots,(a_M,b_M), \tag{15}$$

where $a_i\in\{1,2\}$ and $b_i\in\{1,\ldots,N_b\}$, corresponding to the operators H_{a_i,b_i} in Eqs. (12), or $(a_i,b_i)=(0,0)$, corresponding to the identity operator $H_{0,0}$. For a given sequence S_M the order n then denotes the number of non-$(0,0)$ operators in the sequence. For a nonfrustrated lattice, the number n_2 of off-diagonal operators $(2,b_i)$ in the sequence S_M is always even for nonvanishing contributions, thus yielding a positive definite statistical weight $W(\alpha,S_M)$ in Eq. (14).

With a positive definite expansion, the partition function Z can be stochastically evaluated by importance-sampling in the configuration space (α,S_M). For this purpose an algorithm consisting of two different configuration updates is used. In the first update (diagonal update) the sequence S_M is

traversed from beginning to end, while attempting substitutions $(0,0)\leftrightarrow(1,b_i)$. The substitution $(0,0)\rightarrow(1,b_i)$ is attempted only if the spins connected by bond b_i are antiparallel [for a nonvanishing contribution with the definition of the diagonal operator in Eq. (12a)]. The probabilities to use for accepting/rejecting the change have been given elsewhere, e.g., in Ref. 34. An accepted attempt changes the expansion order n by ±1. If an off-diagonal operator $(2,b_i)$ is encountered no single operator substitution can be carried out, and instead the saved state $|\alpha\rangle$ is updated by flipping the two spins connected by the bond b_i, so that the state on which the diagonal operators act are always available when attempting and update $(0,0)\rightarrow(1,b_i)$. In the second update (operator-loop update) the sequence S_M is uniquely decomposed into a number N_l of operator loops, in which substitutions $(1,b_i)\leftrightarrow(2,b_i)$ can be carried out, independently with probability $1/2$ for each loop. All the spins associated with the loops are also flipped. During the operator-loop update the order n is kept fixed and the weight of the configuration is unchanged. The operator-loop update was introduced and discussed in detail in Ref. 34.

The simulation is started with a random state $|\alpha\rangle$ and an empty sequence $S_M=(0,0),(0,0),\ldots,(0,0)$ of arbitrary (short) length M. One Monte Carlo step (MC step) consists of a diagonal update followed by an operator-loop update. During the equilibration stage of the simulation the cutoff M is adjusted to always exceed the maximum order n reached. Hence, the truncated partition function Z in Eq. (13) is no approximation. Observables are measured after every MC step and expectation values and their errors are determined by the usual method of data binning. Estimators for various observables of the Heisenberg antiferromagnet, in the context of the SSE method, are discussed in Ref. 33. The susceptibility is given in Eq. (3), where the sum is evaluated in the stored state $|\alpha\rangle$. The internal energy and the specific heat are given by[33]

$$E=-\frac{\langle n\rangle}{\beta}, \tag{16a}$$

$$C=\langle n^2\rangle-\langle n\rangle^2-\langle n\rangle. \tag{16b}$$

The operator-loop formulation of the SSE method, as described above, is directly applicable to the isotropic Heisenberg antiferromagnet. Impurities in the form of vacancies, added spins, and missing bonds can be included with only very minor changes in the algorithm. In the added-spin impurity case, the only change in a program for the pure model is that the acceptance probabilities in a diagonal update $(0,0)\rightarrow(1,b_k)$, involving the additional bond k connecting the impurity spin, depend on the bond strength J_k. However, the impurities consisting of a frustrating ferromagnetic bond or four nonfrustrating ferromagnetic bonds necessitate some additional considerations, as will be discussed next.

For a ferromagnetic bond, the diagonal bond operator (12a) is defined as $2(1/4+S_i^zS_j^z)$ and the off-diagonal (12b) is multiplied by −1. During the diagonal update the substitution $(0,0)\rightarrow(1,b_i)$, where b_i is a ferromagnetic (antiferromagnetic) bond, is hence attempted only if the spins connected by bond b_i are parallel (antiparallel). The rules for constructing the operator loops are also modified, as discussed in Ref. 38. For the impurity consisting of four nonfrustrating ferromagnetic bonds, the expression for the statistical weight W in Eq. (14) is still valid if n_2 is replaced by the number n_{A2} of off-diagonal operators $(2,b_i)$ acting on antiferromagnetic bonds. Because of the symmetry of the arrangement of four ferromagnetic bonds, this number also has to be even, and, therefore, the weight W is still positive definite.

A single frustrating ferromagnetic bond (here with coupling $J_F=J$) in the Heisenberg antiferromagnet gives rise to a sign problem. Proceeding as in the case of four ferromagnetic bonds discussed above, the sign would be determined by the number of spin flips of antiferromagnetic bonds, which now can be even or odd. Since the total number of flips still has to be even, we can also define the sign as $(-1)^{n_{F2}}$, where n_{F2} is the number of spin flips on the ferromagnetic bond. However, we can also proceed in a different way which allows for an alleviation of the sign problem by position-averaging when $J_F=J$. We then treat the ferromagnetic bond in the same way as an antiferromagnetic bond in the diagonal update, i.e., a diagonal operator can appear only on antiparallel spins. The sign will then be given by $(-1)^{n_F}$, where n_F is the total number of operators—diagonal and off-diagonal—operating on the ferromagnetic bond. The simulation of the system with a ferromagnetic bond then proceeds exactly as the simulation of the pure antiferromagnet, i.e., expectation values can be calculated using $|W|$ and by reweighting the measurements with the sign $S=(-1)^{n_F}$ of the corresponding configuration,

$$\langle A\rangle=\frac{\langle AS\rangle_{|W|}}{\langle S\rangle_{|W|}}. \tag{17}$$

In practice, however, the calculations become impossible when $\langle S\rangle_{|W|}$ approaches zero. Here a technique based on positional averaging is used to tackle this problem. The idea is to replace the sign S of a given configuration with the averaged sign[39]

$$\Sigma=\frac{1}{N_b}\sum_R S(R), \tag{18}$$

where an average of the sign $S(R)=(-1)^{n_F(R)}$ is taken with respect to all possible locations R of the ferromagnetic bond. Expectation values are then given by

$$\langle A\rangle=\frac{\langle A\Sigma\rangle_{|W|}}{\langle\Sigma\rangle_{|W|}}. \tag{19}$$

This technique was discussed in a more general context in Ref. 39, where it was shown that it significantly alleviates the sign problem of the antiferromagnet with randomly positioned ferromagnetic bonds. This came at the price of an approximation corresponding to switching to an "annealed" disorder. Here, in the single-impurity problem, there is no approximation as the trick simply corresponds to simultaneously studying systems with all possible locations of the

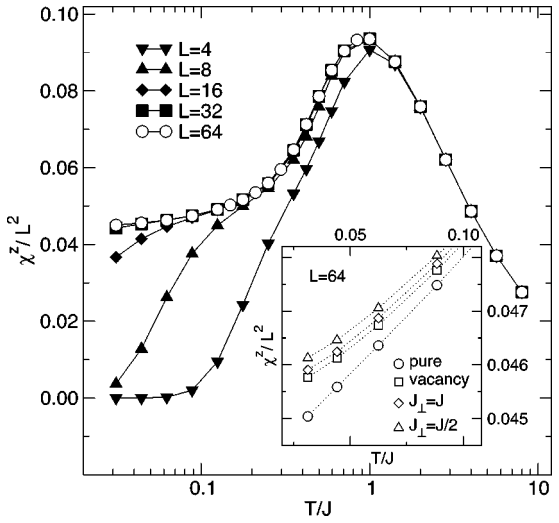

FIG. 4. SSE results for the magnetic susceptibility of the pure 2D Heisenberg antiferromagnet for different system sizes L. Error bars are smaller than the symbols. The inset shows a comparison between the low-T behavior for the pure, vacancy, and added-spin models with $L=64$. For the added-spin model, two values on the coupling constant $J_\perp/J$ are considered.

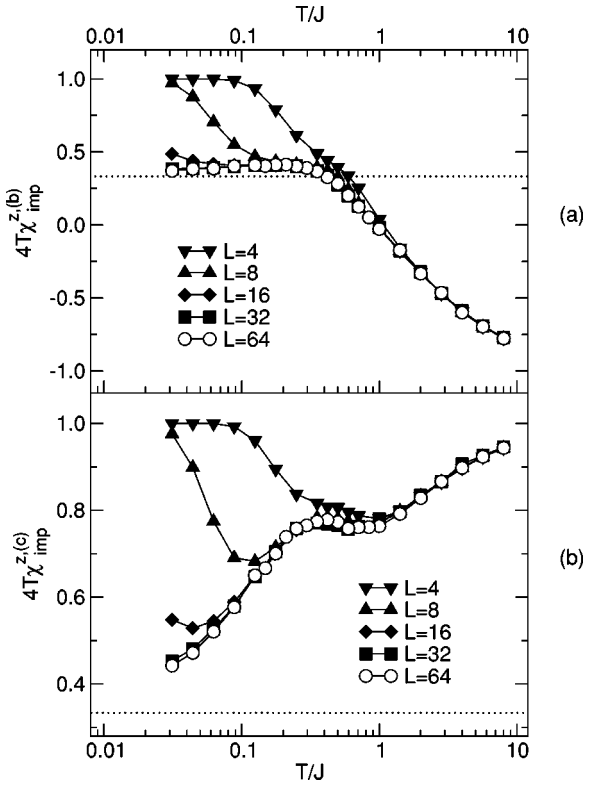

FIG. 5. The impurity susceptibilities of the (a) vacancy and (b) added-spin ($J_\perp=J$) models, for different system sizes L. The dotted lines show the expected asymptotic behavior $4T\chi^z_{\rm imp}\to 1/3$ as $T\to 0$. Error bars are smaller than the symbols.

ferromagnetic bond. When considering only a single position R of the ferromagnetic bond, the sign problem will be more severe than with a redefinition of the diagonal operator discussed above for the four-bond impurity. However, when using the position averaging there will be some system size above which the statistic is improved. We here obtained expectation values with reasonable statistical errors for system sizes up to $L=32$ at temperatures down to $T=J/8$. Since the evaluation of the sign during the simulation is completely separate from the sampling procedures, the effect of a ferromagnetic bond can actually be obtained as a "bonus" while simulating the pure antiferromagnet. A drawback of the position averaging method is that it does not allow for ferromagnetic bond strengths $J_F\neq J$, except perhaps for J_F very close to J where reweighting should work.

We next briefly comment on the accuracy needed to study the impurity effects and the use of improved estimators for increasing the accuracy. For large L, the effect of a single impurity on the magnetic susceptibility χ^z is very small, as shown in the inset of Fig. 4. In order to get acceptable errors for the impurity susceptibilities $\chi^z_{\rm imp}$ in Eq. (2) very precise values for the individual susceptibilities are clearly necessary. To achieve this, an improved estimator[40] is used. The general idea is to reduce the statistical errors by replacing the value of an observable A corresponding to a given Monte Carlo configuration by an estimator $\overline{A_i}$ obtained by averaging over many equal-weight configurations during the operator-loop update. In the case of the susceptibility, this is particularly simple since the magnetization is a conserved quantity. Some of the loops will go through (once or multiple times) the state $|\alpha\rangle$, i.e., the state on which the ordered operator product is acting on in Eq. (13). Defining σ^z_i as the sum over all the spins in $|\alpha\rangle$ covered by the ith loop, we clearly have

$$M^z=\sum_{i=1}^{N} S^z_i \equiv \sum_{i=1}^{N_l}\sigma^z_i. \tag{20}$$

We can now average this over all the 2^{N_l} ways of flipping the loops, giving

$$\chi^z=\beta\left\langle \sum_{i=1}^{N_l}(\sigma^z_i)^2\right\rangle. \tag{21}$$

Figure 4 shows size-normalized results for the magnetic susceptibility obtained this way for the pure 2D Heisenberg antiferromagnet, as well as low-T data for systems with an impurity. We believe that these results are the most accurate ones currently available for this model and therefore also list selected numerical data in the Appendix. For the internal energy and the specific heat, Eqs. (16a) and (16b), no improved estimator of the type discussed above can be constructed. The energy can nevertheless be calculated to high accuracy, as seen in the Appendix. For the specific heat, it is very difficult to reach good accuracy at low temperature. Nevertheless, we are able to clearly discern the expected[41] behavior $C\propto T^2$ at low T, as shown in Fig. 14 in the Appendix.

IV. RESULTS

Here, in Sec. IV A, we begin by presenting susceptibility results for the $S_i\neq 0$ impurities illustrated in Fig. 1. In Sec.

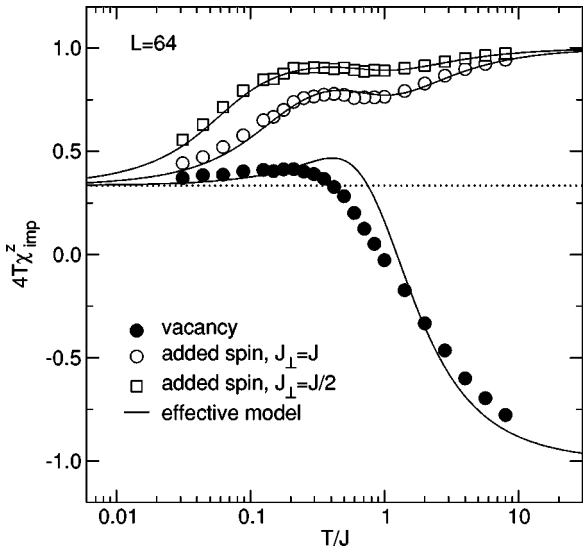

FIG. 6. $L=64$ results for the impurity susceptibilities of the vacancy and added-spin models is compared to the results of the corresponding effective models. The dotted line shows the value $1/3$.

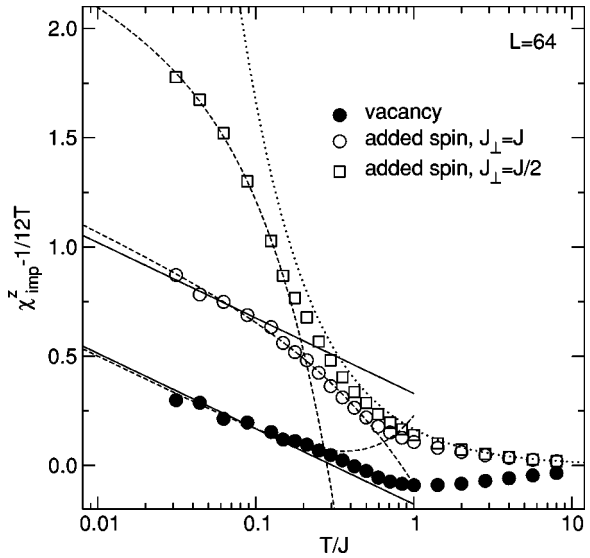

FIG. 7. SSE data for $\chi^z_{\rm imp}-1/12T$ of the vacancy and added-spin models with system sizes $L=64$. Straight lines and dashed curves are fits of the theoretical results in Ref. 28 to our low-T simulation data. The dotted curve shows the $1/6T$ behavior.

IV B we consider the case of a vacancy in a 3D system, and in Sec. IV C we look at the system with two vacancies. We discuss results for the $S_i=0$ bond impurities (Fig. 2) in Sec. IV D. In Sec. IV E we summarize our results for the impurity effects on the energy and the specific heat.

A. $S_i \neq 0$ impurities

The impurity susceptibilities for a vacancy and an added spin with $J_\perp=J$ are shown in Figs. 5(a) and 5(b), respectively. The results are multiplied by $4T$. At high T the data for different system sizes L coincide, while at lower T finite-size effects are clearly seen for $L\leqslant 16$. The finite-size effects are due to the $S=1/2$ ground states of the vacancy and added-spin models, to which the system converges below an L dependent crossover temperature, as has recently been discussed by Sushkov.[29] For the largest system size considered here, $L=64$, all finite-size effects are eliminated within statistical errors for temperatures down to $T/J=1/32$. The observed behavior at high T for both impurity types is due to the fact that the total susceptibility is then just the sum of the Curie contributions of each independent spin, i.e.,

$$\chi^{z,(b,c)}_{\rm imp}=\chi^z_{(b,c)}-\chi^z_{(a)}\rightarrow\frac{L^2\mp 1}{4T}-\frac{L^2}{4T}=\mp\frac{1}{4T} \qquad (22)$$

as $T\rightarrow\infty$. The minus (plus) sign is for the vacancy (added-spin) impurity model. According to the expression in Eq. (1), the leading order behavior of the impurity susceptibility is $4T\chi^z_{\rm imp}\sim 4S_i^2/3$ as $T\rightarrow 0$. For a $S_i=1/2$ impurity, the constant value $1/3$ should then be approached at low T. This is also clearly observed in the size-converged ($L=64$) data for the vacancy impurity, shown in Fig. 5(a). For the added-spin impurity shown in Fig. 5(b), an approach of $4T\chi^{z,(c)}_{\rm imp}$ to $1/3$ is also likely, although the convergence occurs at lower T than for the vacancy. At intermediate T the results for the two different impurity types are strikingly different. Specifically, the shoulderlike structure with a minimum around $T/J\approx 0.8$ observed in the added-spin data has no counterpart in the vacancy data, but in both cases there is a maximum at $T/J\approx 0.2$. Some of the differences clearly are related to the different $T\rightarrow\infty$ behaviors.

In Fig. 6 the size-converged SSE data are compared with the results of the effective models. Results are also shown for the added-spin impurity with $J_\perp=J/2$. The values of the two parameters of the effective models, $\alpha/J=2.25$ and $r/J=1.90$,[37] were chosen for optimal overall agreement between the SSE data and the effective model results, for both the vacancy and the added-spin systems. For this choice of values, the effective models reproduce the added-spin data with a remarkable precision down to $T/J\approx 0.1$, for both $J_\perp=J$ and $J_\perp=J/2$. Moreover, with the same set of values a reasonable agreement is also obtained for the vacancy system. Hence, the same parameters describe well a wide range of coupling strengths to the added spin (the vacancy corresponds to $J_\perp/J=\infty$).

In each of the three cases shown in Fig. 6, the effective models also reproduce the low-T leading-order behavior suggested in Eq. (1), i.e., $4T\chi^z_{\rm imp}\sim 4S_i^2/3=1/3$ for a $S_i=1/2$ impurity. Hence, the effective models clearly contain the dominant impurity physics and are able to distinguish between different impurity types in a broad T range. In analogy with the results for the effective models, the observed low-T leading-order behavior of the full Heisenberg models is ascribed to a susceptibility component parallel to a locally Néel ordered domain coupled to the impurity, i.e., $(1/3)\chi^{\parallel,(i)}_{\rm imp}\sim S_i^2/3T=1/12T$, where $i=b,c$, and $S_i=1/2$.

We next examine the thermodynamic low-T impurity susceptibilities more closely by subtracting from them the leading-order term $S_i^2/3T$. The resulting quantities should then describe the transverse impurity susceptibilities at low T, i.e., $(2/3)\chi^{\perp,(i)}_{\rm imp}\sim\chi^{z,(i)}_{\rm imp}-S_i^2/3T$.[30] The results in Fig. 7 for $\chi^{z,(b,c)}_{\rm imp}-1/12T$ of the vacancy impurity, and of the added-

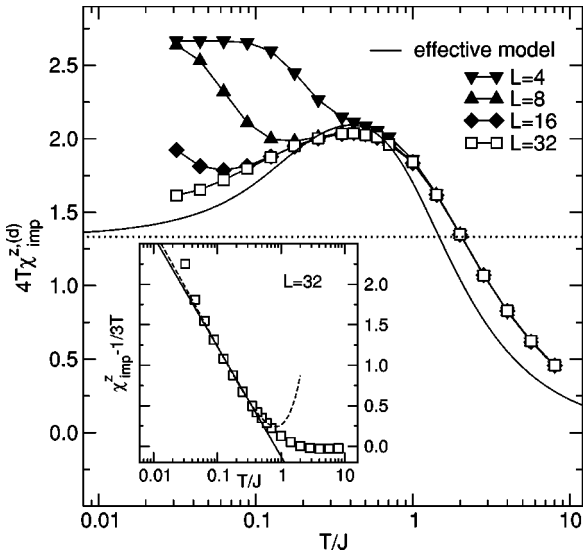

FIG. 8. Impurity susceptibilities for different system sizes L of the impurity model with four ferromagnetic bonds. The solid curve shows the result of the corresponding effective model, which assumes the asymptotic value $4/3$ (shown by the dotted line) at low T. The log divergent behavior of $\chi^z_{\rm imp}-1/3T$, for a system of size $L=32$, is shown in the inset, where the solid line and the dashed curve are fits of the theoretical results in Ref. 28 to our low-T simulation data.

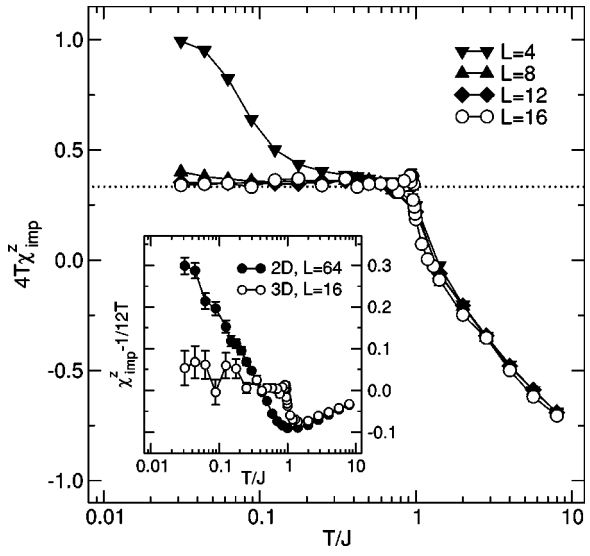

FIG. 9. The impurity susceptibilities of the 3D Heisenberg antiferromagnet with a vacancy, for different system sizes L. The dotted line shows the value $1/3$. A comparison between $\chi^z_{\rm imp}-1/12T$ of the 2D and 3D models is shown in the inset.

spin impurity with $J_\perp=J$, show an apparent logarithmically divergent behavior as $T\to 0$. The results for the added-spin impurity with $J_\perp=J/2$ are not conclusive in this regard, but a similar log divergent behavior at still lower temperatures is clearly plausible. As $J_\perp/J\to\infty$, the magnetic properties of the added-spin model should become equivalent to those of the vacancy model. In the limit $J_\perp/J\to 0$, on the other hand, the added spin is decoupled from its host and the impurity susceptibility becomes simply the susceptibility of a single spin $(1/4T)$, i.e., $\chi^z_{\rm imp}-1/12T\sim 1/6T$. When comparing the SSE results in Fig. 7 with each other, it then seems that the log divergent behavior starts at higher T as the magnitude of the coupling to the added spin, $J_\perp/J$, is increased. This can be naturally understood as an impurity moment strongly coupled to the environment can develop only at T below $J_\perp$.

According to the theoretical expression by Sachdev and Vojta,[28] Eq. (1), the slopes of the the low-T curves should be equal on the log-linear scale used in Fig. 7. The slope is given by $S_i^2/3\pi\rho_s$, where S_i is the "bare" impurity spin and ρ_s is the spin stiffness of the bulk-ordered antiferromagnet, for which we use the value $\rho_s/J=0.181$.[42] Our results for the vacancy and the $J_\perp=J$ added spin are indeed consistent with this prediction. The straight solid lines are fits of the leading logarithmic part, $\propto\ln(C_1\rho_s/T)$, of Eq. (1) to the low-T data, whereas the dashed curves show fits including also the subleading correction $\propto T\ln(C_2\rho_s/T)$. For the vacancy system we find $C_1\approx 1.7$ (in the leading-order fit) or $C_1\approx 1.6$ and $C_2\approx 0.3$, for the added-spin system $(J_\perp=J)$ $C_1\approx 50$ or $C_1\approx 73$ and $C_2\approx 184$. For the added-spin impurity with $J_\perp=J/2$, no fit can be made with only the leading term, and we find $C_1\approx 10^5$ and $C_2\approx 10^{19}$.

Results for the impurity model with a configuration of four ferromagnetic bonds are shown in Fig. 8. Again, the results for different L coincide at high T, while finite-size effects are seen at lower T. The high-T observed behavior, $4T\chi^{z,(d)}_{\rm imp}\to 0$ as $T\to\infty$, is due to the fact that the susceptibilities of the doped and the pure models cancel, since there is an equal number of independent spins in both models at high temperatures. The ground state spin of this model is $S=1$, and hence also an impurity moment $S_i=1$ can be anticipated. The low-T finite-size susceptibility should then be $4T\chi^z\sim 4T[S(S+1)/3T]=8/3$ and in the thermodynamic limit $4T\chi^z\sim 4T(S^2/3T)=4/3$. This behavior is indeed seen in Fig. 8; for $L=4$ and 8 the low-T behavior dictated by the ground state spin can be observed, while for $L=32$ the low-T susceptibility is size-converged at least to $T/J=1/16$ and is consistent with a convergence to $4/3$. We also show results for the corresponding effective model. Using the same values for α/J and r/J as previously for the vacancy and added-spin effective models, changing only the sign of α, the behavior agrees qualitatively with the SSE results. The inset of Fig. 8 shows $\chi^{z,(d)}_{\rm imp}-1/3T$, which at low T should be dominated by the transverse component $(2/3)\chi^{\perp,(d)}_{\rm imp}$. Again, an apparent log divergent trend is observed. The straight line and the dashed curve are fits of Eq. (1). Data for the two lowest T are not included in these fit because of the finite-size effects that most likely remain here. Nevertheless, the results support the universal low-T prefactor (slope) of the leading logarithmic correction.

B. Vacancy in a 3D system

Here we discuss the case of a vacancy in the 3D Heisenberg antiferromagnet. Some predictions[28] were recently made also for this system, but since we have not achieved sufficient accuracy they are not tested in detail here. The leading-order behavior can nevertheless be extracted. In Fig. 9 the SSE data are shown for different system sizes

L ($N=L3$), and a comparison between the 3D and 2D data is shown in the inset. The high-T behavior, as well as the low-T finite-size effects, have the same explanations as those given for the 2D results. For the largest system size, $L=16$, most finite-size effects are eliminated within statistical errors in the T range considered. The observed thermodynamic behavior is reminiscent of the 2D results in Fig. 5(a), with the exception that the transition to a constant-valued behavior now occurs abruptly at $T/J \approx 0.95$, which is the Néel temperature T_N of the model.[35] There are signs of a singular behavior of the impurity susceptibility at the transition. At temperatures $T \leqslant T_N$, the susceptibility is seen to follow very closely the proposed[21,28] behavior $S^2/3T$. It should be noted that although 3D order sets in below T_N, our finite-size systems nevertheless do not break the symmetry and the direction of the Néel vector is not fixed. In an infinite symmetry-broken system, the $S^2/3T$ behavior would not be present if the magnetization fluctuations are defined with respect to the average in the direction of the fixed Néel vector.

In the inset of Fig. 9, the perpendicular component $(2/3)\chi^{\perp}_{\mathrm{imp}} = \chi^{z}_{\mathrm{imp}} - (1/3)\chi^{\parallel}_{\mathrm{imp}}$ is compared to the analogous quantity of the 2D model. Although the statistical accuracy is not very high at low temperature, it is clear that the behaviors are different. The 3D results do not indicate any log divergent behavior of the type observed in the 2D system. Instead an almost constant behavior is observed, as also predicted in the field theory.[28]

C. Two vacancies in 2D

Next we present SSE results for the 2D Heisenberg antiferromagnet with two vacancies on different sublattices. The results for the impurity susceptibility are multiplied by a factor $1/2$, so that single-impurity values should be obtained when the correlation length is much shorter than the separation between the vacancies. When T is lowered, interactions between the impurities become important as the correlation length ξ grows exponentially. At T corresponding to a correlation length of the same order as the vacancy separation, the moments due to the two vacancies on different sublattices are pinned by the local Néel order antiparallel to each other, resulting in a rapid quenching of the parallel component of the impurity susceptibility. Hence, χ^{z}_{imp} does not diverge as $T \to 0$. The data shown in Fig. 10(a) is for the case of maximum separation of two vacancies on different sublattices; $\mathbf{r} = (L/2-1, L/2)$. Since ξ diverges exponentially as $T \to 0$, the point at which χ^{z}_{imp} deviates from the divergent single-vacancy behavior moves only very slowly to lower T as L is increased. For larger L, an almost constant χ^{z}_{imp} is observed. However, no sign of convergence of the plateau value is seen. Clearly, in a system of finite size there will always be some interaction also between the perpendicular components of the two vacancies, and hence even for large L the two-vacancy model does not trivially reproduce the single-vacancy results below some temperature. It is plausible, however, that the roughly $\ln(L)$ divergence of the plateau height seen in Fig. 10(a) continues as $L \to \infty$. This would be fully in line with the log divergent $\chi^{\perp,(b)}_{\mathrm{imp}}$ for the single vacancy.

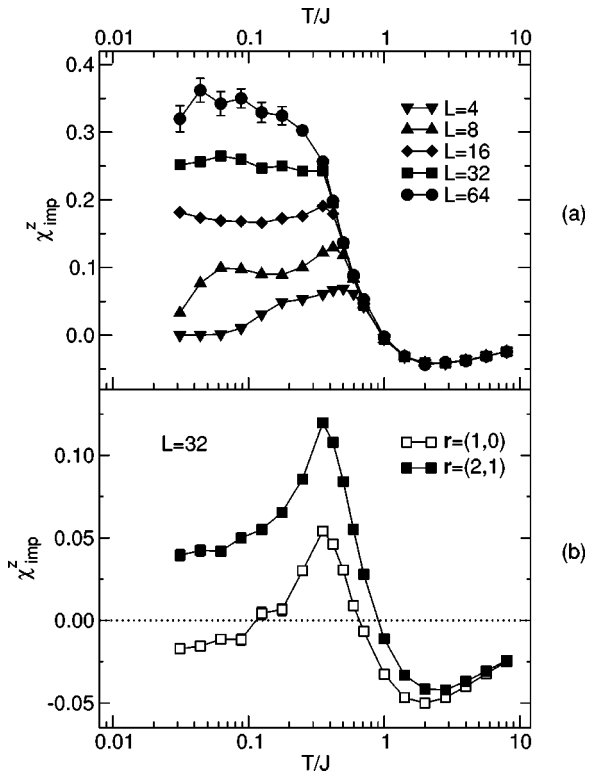

FIG. 10. Impurity susceptibility for different system sizes L of the square lattice with two vacancies. The vacancies are as far apart as possible in (a). In (b) the $L=32$ results are shown for the cases when the two vacancies are nearest neighbors (open symbols) and at distance $\mathbf{r}=(2,1)$ from each other (solid symbols).

The very sudden crossover from divergent to almost T independent behavior seen in Fig. 10(a) speaks for a component $\chi^{\perp,(i)}_{\mathrm{imp}}$ aligning strongly to the local Néel order (which becomes the global order at the L dependent crossover temperature), and justifies the separation into parallel and transverse (with respect to the local fluctuating Néel vector) impurity susceptibility components already at intermediate T. However, the longitudinal component is not strictly $S^2_i/3T$; the recent field theory by Sachdev and Vojta predicts that the remaining longitudinal contributions, once this leading term has been subtracted, has a temperature dependence $\propto T \ln(1/T)$. Nevertheless, the transverse contribution, which is $\propto \ln(1/T)$ at low T, dominates.

In Fig. 10(b), SSE data is shown for the case of the two vacancies being nearest neighbors, $\mathbf{r}=(1,0)$, as well as at separation $\mathbf{r}=(2,1)$ on the square lattice. Again, the single-vacancy data are reproduced at high T. In contrast to the divergent trend seen in the maximum-separation data in Fig. 10(b), the finite-size behavior has now converged to a near constant at low T, and no signs of a log divergence as a function of L is observed. In the figure we show only $L=32$ results, which are almost converged to the thermodynamic limit. The absence of log corrections for two vacancies at fixed separation is consistent with results of a Green's function calculation,[16] where the introduction of a second extra spin destroyed the log divergence in the frequency dependent $T=0$ susceptibility observed for the system with a single extra spin.

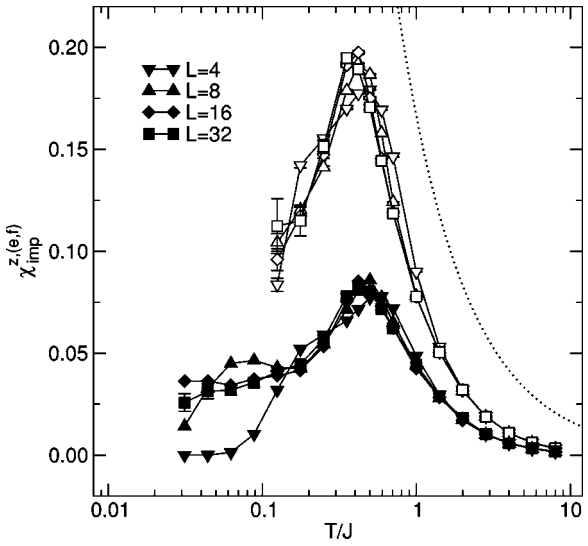

FIG. 11. Impurity susceptibilities for different system sizes L of the models with a missing bond (solid symbols) and a ferromagnetic bond with $J_F=J$ (open symbols). The dotted curve shows the expected high-T behavior $1/6T$ for large J_F/J.

D. $S_i=0$ impurities

We next turn to the QMC results shown in Fig. 11 for the 2D Heisenberg antiferromagnet with a ferromagnetic bond or a missing bond, i.e., with $J_F=J$ or $J_F=0$, respectively. In this case the impurity susceptibilities do not diverge as $T\to 0$, and the results are not, therefore, multiplied with T. The observed high-T behavior of each model, $\chi^z_{\mathrm{imp}}\to 0$, is due to the fact that the susceptibilities of the pure and the doped models cancel, since there is an equal number of independent spins in both models at high temperatures. For the missing-bond impurity, low-T finite-size effects are clearly seen for $L=4$ and 8, while for the largest system size $L=32$, the results should be almost size-converged and show little temperature dependence at low T. The observed finite-size behavior, $\chi^z_{\mathrm{imp}}(T\to 0)\to 0$ reflects the $S=0$ ground state, and clearly the size-converged T dependence also speaks for an $S_i=0$ impurity. Results for the ferromagnetic-bond impurity are limited to temperatures down to $T/J=1/8$, because of the sign problem caused by the frustrating ferromagnetic bond. The data are reminiscent of the missing-bond results, and hence also the ferromagnetic-bond impurity has $S_i=0$. Both models are, clearly, special cases of the system with one ferromagnetic bond of arbitrary strength J_F. It would be interesting to investigate how the impurity spin magnitude S_i changes as J_F is increased. For $J_F/J\gg 1$, the two spins connected by the ferromagnetic bond form a triplet and hence should give an $S_i=1$ Curie contribution $S_i(S_i+1)/3T=2/3T$ when $J\lesssim T\lesssim J_F$. The remaining $N-2$ spins each contribute $1/4T$, and hence the impurity susceptibility should be $1/6T$ in this regime. In Fig. 11 the results for $T>J$ are closer to this form for $J_F=J$ than for $J_F=0$, but the requirement $J<T<J_F$ is not satisfied and the deviations (reduction relative to $1/6T$) reflect an expected crossover from the high-T independent-spin form $\chi^z_{\mathrm{imp}}\approx 0$.

An interesting question is whether the classical-like Curie behavior $\chi^z_{\mathrm{imp}}\approx S_i^2/3T$ with $S_i=1$ can be observed in this model for $J_F>J$. As already discussed in Sec. II, the asymmetric coupling to the bulk of the two spins connected by the ferro bond most likely implies a $T\to 0$ behavior corresponding to $S_i=0$ for any finite J_F. This is because an $S_i=1$ impurity requires that the two spins at the ferro bond are dominantly in the $m^z=1$ state $|\uparrow\uparrow\rangle$ with respect to the local Néel order (in a semiclassical picture such as our effective impurity model), whereas in fact the couplings in this case instead favor the $m^z=0$ component $(|\uparrow\downarrow\rangle+|\downarrow\uparrow\rangle)/\sqrt{2}$.[17]

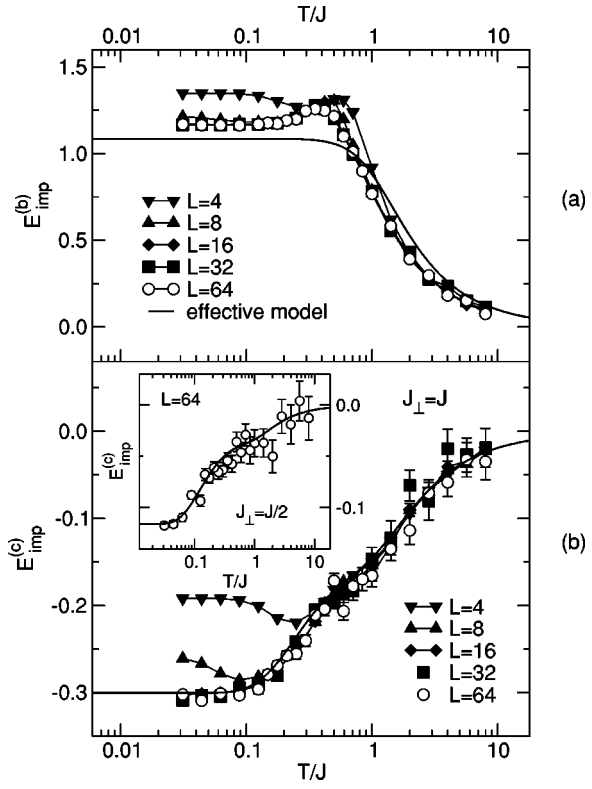

FIG. 12. The impurity energies of the (a) vacancy and (b) added-spin ($J_\perp=J$) models, for different system sizes L. The inset shows the $L=64$ QMC results for the added-spin model with $J_\perp=J/2$. The curves are results of the corresponding effective models.

E. Internal energy and specific heat

We finally discuss our SSE calculations concerning impurity effects on the internal energy and the specific heat, which we have obtained using the estimators in Eqs. (16a) and (16b), respectively. In analogy to Eq. (2), we again define the impurity quantities as differences between the doped and the pure systems, i.e.,

$$E^{(i)}_{\mathrm{imp}}=E_{(i)}-E_{(a)}, \tag{23a}$$

$$C^{(i)}_{\mathrm{imp}}=C_{(i)}-C_{(a)}, \tag{23b}$$

where $i=b,c,d,e$, and f, correspond to the different impurity systems shown in Figs. 1 and 2, and the symbol a denotes the pure system. In Fig. 12 results for the impurity energies are shown for the vacancy model (a) and the added-spin model (b) with $J_\perp=J$ and $J_\perp=J/2$ (shown in the inset). At

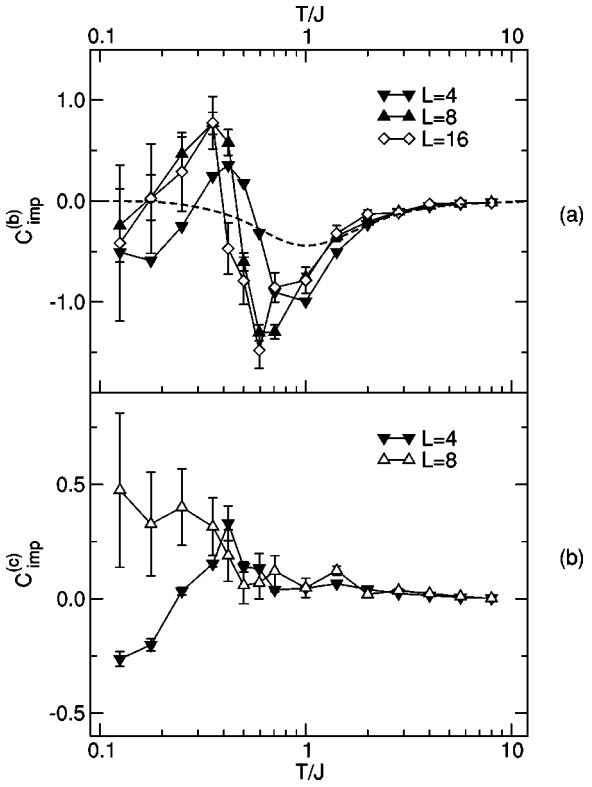

FIG. 13. The impurity specific heats of the (a) vacancy and (b) added-spin ($J_\perp = J$) models, for different system sizes L. The dashed curve in (a) shows the result of the effective model.

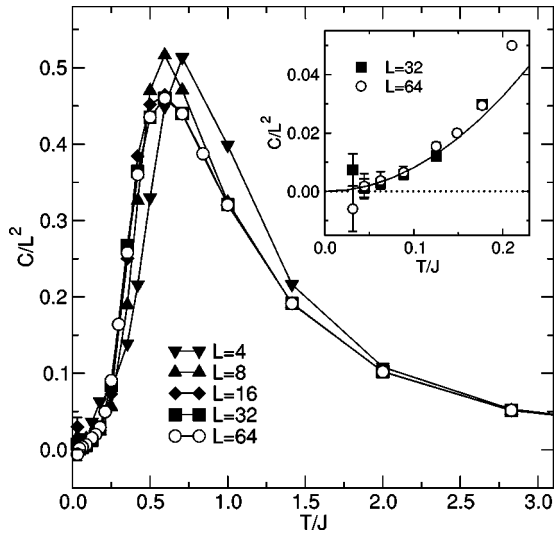

FIG. 14. Size-normalized specific heats of the pure 2D Heisenberg antiferromagnet for different system sizes L. Error bars are smaller than the symbols. The inset compares our low-T data with theory (solid curve) (Ref. 41).

high T the impurity energies vanish, since the mean energy of each independent spin becomes zero. For $L=64$, all finite-size effects are eliminated within statistical errors for both models in the T range considered. Since the vacancy system has four antiferromagnetic bonds less than the pure system, the impurity energy $E^{(b)}_{\rm imp}$, shown in Fig. 12(a), is positive at all T. At low T the results converge to a constant value, which should be equal to the energy cost of removing one spin from an infinite lattice in its ground state. The low-T value observed in Fig. 12(a) is indeed consistent with $T=0$ results obtained in a previous linear spin-wave study.[15] Results for the added-spin model with $J_\perp = J$, shown in Fig. 12(b), are negative because of the one extra antiferromagnetic bond, and the size-converged behavior seems to also tend to a constant as $T \to 0$. This constant value corresponds to the energy cost of removing the off-plane added spin from its host lattice, and its magnitude is observed to be roughly one-fourth of the low-T value of the vacancy impurity energy. The T dependence of the $L=64$ results for the added-spin impurity with $J_\perp = J/2$, shown in the inset, are qualitatively very similar, but because of the smaller impurity-bond strength the absolute values are smaller.

The solid curves in Fig. 12 are results of the corresponding effective models. Using the same values on α/J and r/J as previously when calculating the impurity susceptibilities, we obtain a qualitative agreement for the vacancy model while the agreement is remarkably good for the added-spin model, both for $J_\perp = J$ and $J_\perp = J/2$ (inset). Hence, in addition to reproducing the impurity susceptibilities of the full models, the effective models also describe properly the energetics of the full models. Also, the parameters α and r can be tuned to give a better agreement for the vacancy model in Fig. 12(a), but this in turn will give a poorer agreement between QMC and effective-model results for the impurity susceptibility of the vacancy model in Fig. 6.

In Fig. 13 QMC results for the impurity specific heats are shown for the vacancy model (a) and the added-spin model (b) with $J_\perp = J$. As the system size is increased and the temperature is lowered the statistical errors grow rapidly. The size-converged behavior is difficult to determine below $T/J \approx 0.3$, but $C^{(b)}_{\rm imp}$ in Fig. 13(a) is, nevertheless, consistent with the behavior of $E^{(b)}_{\rm imp}$ in Fig. 12(a), as $C = dE(T)/dT$. The point at which $C^{(b)}_{\rm imp}$ goes through zero, $T/J \approx 0.5$, corresponds to the maximum in the energy curve $E^{(b)}_{\rm imp}$ in Fig. 12. The effective model reproduces well the high-T behavior and also exhibits a negative minimum at intermediate temperature. However, this feature is much less pronounced than for the full model, and the maximum at lower T is missing. In Fig. 12(b), sufficient accuracy in the simulations has not been reached for larger system sizes, and the size-converged behavior can therefore not be determined.

V. SUMMARY

In this paper we have presented results of an extensive QMC study of impurity effects in the $S=1/2$ Heisenberg antiferromagnet on a square lattice, as well as some results for a 3D system. The effects of different types of single static impurities on the magnetic susceptibility and the specific heat have been investigated.

For several types of $S_i \neq 0$ impurities in 2D (vacancy, added spin, ferromagnetically coupled spin), our very precise simulation data has revealed an additive logarithmic correction to the predicted classical-like Curie contribution $S_i^2/3T$

TABLE I. Selected $L=64$ data for $\chi^z_{(i)}/L^2$ at inverse temperature J/T, where $i=a,b$, and c correspond to the pure, vacancy, and added-spin systems, respectively.

			$i=c$	
J/T	$i=a$	$i=b$	$J_\perp=J$	$J_\perp=J/2$
32	0.045043(3)	0.045767(4)	0.045907(4)	0.046128(3)
16	0.046359(3)	0.046737(3)	0.046867(3)	0.047056(3)
8	0.049144(3)	0.049344(3)	0.049461(2)	0.049557(3)
4	0.055994(1)	0.056092(1)	0.056179(1)	0.056214(1)
2	0.0786001(4)	0.0786347(4)	0.0786945(4)	0.0787106(4)
1	0.0935393(2)	0.0935377(2)	0.0935859(2)	0.0935937(2)

TABLE II. Selected $L=64$ data for $-E_{(i)}/L^2$ at inverse temperature J/T, where $i=a,b$, and c correspond to the pure, vacancy, and added-spin systems, respectively.

			$i=c$	
J/T	$i=a$	$i=b$	$J_\perp=J$	$J_\perp=J/2$
32	0.6694416(5)	0.6691562(5)	0.6695154(6)	0.6694702(5)
16	0.6693890(7)	0.6691048(7)	0.6694625(7)	0.6694158(7)
8	0.6689102(9)	0.6686247(8)	0.668983(1)	0.6689330(9)
4	0.663745(1)	0.663452(1)	0.663807(1)	0.663761(1)
2	0.593051(1)	0.592755(1)	0.593093(1)	0.593060(2)
1	0.387560(2)	0.387372(2)	0.387600(2)	0.387569(2)

to the impurity susceptibility. We have argued that this logarithmic contribution reflects primarily fluctuations transverse to the local Néel order at the impurity. This is in agreement with recent field-theoretical work,[28,29] carried out after our initial report of log corrections.[27] Here we have shown that our numerical results are in excellent quantitative agreement with these field-theoretical results,[28,29] containing both leading and subleading logarithmic corrections. In 3D, we find no signs of logarithmic corrections, in accord with predictions.[28]

In order to have a simple mechanism explaining the leading-order (i.e., apart from the log corrections) impurity physics, we have also introduced few-spin effective models. Comparisons with the QMC results show that the effective models can distinguish between impurities of different types and spins S_i. In many cases the quantitative agreement between the effective and full models is surprisingly good over a wide temperature range. This suggests that extended effective models based on larger clusters of spins, e.g., 3×3 clusters centered around the site impurities, should give very accurate descriptions, perhaps also for the vacancy model which we here found was the hardest case to describe with the simplest effective model.

ACKNOWLEDGMENTS

We are grateful to Subir Sachdev and Oleg Sushkov for very valuable discussions. This work was supported by the Academy of Finland, Project No. 26175.

APPENDIX: SELECTED QMC DATA FOR THE SUSCEPTIBILITY, ENERGY, AND SPECIFIC HEAT

The numerical data underlying the analyses carried out in this paper are of very high accuracy—the small errors are only statistical in nature—and may hence be useful as benchmarks for alternative calculations. In Tables I and II we therefore list $L=64$ data for the susceptibility and the internal energy, at several inverse temperatures J/T, for the pure (a), vacancy (b), and added-spin models (c).

In Fig. 14 we show the SSE results for the specific heat of the pure 2D Heisenberg antiferromagnet at temperatures down to $T/J=1/32$. At such low temperatures the specific heat has not been determined reliably in previous studies.[43] We have obtained the results using the direct estimator, Eq. (16b). The low-T data shown in the inset of Fig. 14 are clearly consistent with the quadratic T behavior suggested in the Hasenfratz-Niedermeyer chiral perturbation theory:[41]

$$C(T)=\frac{6\zeta(3)}{\pi c^2}T^2+O(T^4), \tag{A1}$$

where we use $c=1.66$ for the spin-wave velocity[44] and $\zeta(3)=1.2020569$.

[1] E. Manousakis, Rev. Mod. Phys. **63**, 1 (1991); M. A. Kastner, R. J. Birgeneau, G. Shirane, and Y. Endoh, *ibid.* **70**, 897 (1998).
[2] A. Aharony, R. J. Birgeneau, A. Coniglio, M. A. Kastner, and H. E. Stanley, Phys. Rev. Lett. **60**, 1330 (1988).
[3] S.-W. Cheong, A.S. Cooper, L. W. B. Batlogg, J. D. Thompson, and Z. Fisk, Phys. Rev. B **44**, 9739 (1991); S. T. Ting, P. Pernambuco-Wise, J. E. Crow, E. Manousakis, and J. Weaver, *ibid.* **46**, 11772 (1992); M. Corti, A. Rigamonti, F. Tabak, P. Caretta, F. Licci, and L. Raffo, *ibid.* **52**, 4226 (1995); P. Carretta, A. Rigamonti, and R. Sala, *ibid.* **55**, 3734 (1997).
[4] O. P. Vajk, P. K. Mang, M. Greven, P. M. Gehring, and J. W. Lynn, Science **295**, 1691 (2002).
[5] M. Takigawa, N. Motoyama, H. Eisaki, and S. Uchida, Phys. Rev. B **55**, 14129 (1997).
[6] M. Azuma, Y. Fujishiro, M. Takano, M. Nohara, and H. Takagi, Phys. Rev. B **55**, R8658 (1997).
[7] A. H. Castro Neto, E. Novais, L. Borda, G. Zaránd, and I. Affleck, Phys. Rev. Lett. **91**, 096401 (2003).
[8] S. Eggert and I. Affleck, Phys. Rev. B **46**, 10866 (1992).
[9] J. Igarashi, T. Tonegawa, M. Kaburagi, and P. Fulde, Phys. Rev. B **51**, 5814 (1995).
[10] M. Nishino, H. Onishi, P. Roos, K. Yamaguchi, and S. Miyashita, Phys. Rev. B **61**, 4033 (2000).
[11] M. Nishino, H. Onishi, K. Yamaguchi, and S. Miyashita, Phys. Rev. B **62**, 9463 (2000).
[12] H. Fukuyama, N. Nagaosa, M. Saito, and T. Tanimoto, J. Phys.

Soc. Jpn. **65**, 2377 (1996).
[13] A. W. Sandvik, E. Dagotto, and D. J. Scalapino, Phys. Rev. B **56**, 11701 (1997).
[14] G. B. Martins, M. Laukamp, J. Riera, and E. Dagotto, Phys. Rev. Lett. **78**, 3563 (1997).
[15] N. Bulut, D. Hone, and D. J. Scalapino, and E. Y. Loh, Phys. Rev. Lett. **62**, 2192 (1989).
[16] N. Nagaosa, Y. Hatsugai, and M. Imada, J. Phys. Soc. Jpn. **58**, 978 (1989).
[17] P. Schlottmann, J. Appl. Phys. **75**, 5532 (1994).
[18] V. N. Kotov, J. Oitmaa, and O. Sushkov, Phys. Rev. B **58**, 8495 (1998); **58**, 8500 (1998).
[19] N. Nagaosa and T.-K. Ng, Phys. Rev. B **51**, 15588 (1995).
[20] O. P. Sushkov, Phys. Rev. B **62**, 12135 (2000).
[21] S. Sachdev, C. Buragohain, and M. Vojta, Science **286**, 2479 (1999); M. Vojta, C. Buragohain, and S. Sachdev, Phys. Rev. B **61**, 15152 (2000).
[22] S. Sachdev, M. Troyer, and M. Vojta, Phys. Rev. Lett. **86**, 2617 (2001).
[23] S. Eggert and I. Affleck, Phys. Rev. Lett. **75**, 934 (1995).
[24] S. Eggert and S. Rommer, Phys. Rev. Lett. **81**, 1690 (1998); S. Rommer and S. Eggert, Phys. Rev. B **59**, 6301 (1999).
[25] S. Fujimoto and S. Eggert, Phys. Rev. Lett. **92**, 037206 (2004).
[26] K. Murayama and J. Igarashi, J. Phys. Soc. Jpn. **66**, 1157 (1996).
[27] K. H. Höglund and A. W. Sandvik, Phys. Rev. Lett. **91**, 077204 (2003).
[28] S. Sachdev and M. Vojta, Phys. Rev. B **68**, 064419 (2003).
[29] O. P. Sushkov, Phys. Rev. B **68**, 094426 (2003).
[30] A separation of the impurity susceptibility in components parallel and perpendicular to the Néel order is of course strictly applicable only at $T=0$, i.e., when the spin-rotation symmetry is broken. It is nevertheless a useful concept also when the impurity is coupled to a large ordered domain with slow dynamics. However, the exact way in which the separation into longitudinal and transverse components is done is to some extent a matter of calculational definitions outside the limit $T=0$.
[31] A. B. Harris and S. Kirkpatrick, Phys. Rev. B **16**, 542 (1977).
[32] A. L. Chernyshev, Y. C. Chen, and A. H. Castro Neto, Phys. Rev. B **65**, 104407 (2002).
[33] A. W. Sandvik, Phys. Rev. B **56**, 11678 (1997).
[34] A. W. Sandvik, Phys. Rev. B **59**, R14157 (1999).
[35] A. W. Sandvik, Phys. Rev. Lett. **80**, 5196 (1998).
[36] S. Chakravarty, B. I. Halperin, and D. R. Nelson, Phys. Rev. Lett. **60**, 1057 (1988).
[37] We here use slightly different values for α and r than previously in Ref. 27, in order to optimize the agreement between QMC and effective model results for both the susceptibility and the energy, as well as to get a good agreement also in the case of the added-spin model with $J_\perp = J/2$. The results for the vacancy and the added spin with $J_\perp = J$ change very little from those in Ref. 27.
[38] P. Henelius and A. W. Sandvik, Phys. Rev. B **62**, 1102 (2000).
[39] A. W. Sandvik, Phys. Rev. B **50**, 15803 (1994).
[40] H. G. Evertz, Adv. Phys. **52**, 1 (2003).
[41] P. Hasenfratz and F. Niedermayer, Z. Phys. B: Condens. Matter **92**, 91 (1993).
[42] A. W. Sandvik, Phys. Rev. B **66**, 024418 (2002).
[43] J.-K. Kim and M. Troyer, Phys. Rev. Lett. **80**, 2705 (1998); J. Jaklič and P. Prelovšek, *ibid.* **77**, 892 (1996); G. Gomez-Santos, J. D. Joannopoulos and J. W. Negele, Phys. Rev. B **39**, 4435 (1989).
[44] An accurate value of the spin-wave velocity $c=\sqrt{\rho_s/\chi_\perp}$ is obtained from the stiffness $\rho_s \approx 0.181$ calculated in Ref. 42 and the perpendicular susceptibility $\chi_\perp \approx 0.0659$ obtained by O. F. Syljuåsen and A. W. Sandvik, Phys. Rev. E **66**, 046701 (2002).